Modeling colloid transport and retention in saturated porous media under unfavorable attachment conditions

Scott A. Bradford,[1] Saeed Torkzaban,[2] and Jiri Simunek[2]

[1]   A mathematical model is presented for colloid transport and retention in saturated porous media under unfavorable attachment conditions. The model accounts for colloid transport in the bulk aqueous phase and adjacent to the solid surface, and rates of colloid collision, interaction, release, and immobilization on the solid phase. Model parameters were estimated using (1) filtration theory; (2) calculated interaction energies in conjunction with the Maxwellian kinetic energy model of diffusion; (3) information about the velocity magnitude and distribution adjacent to the solid phase that was obtained from pore scale water flow simulations; (4) colloid and collector sizes; (5) the balance of applied hydrodynamic and resisting adhesive torques; and (6) time dependent filling of retention locations using a Langmuirian approach. The presented theory constrains the model parameters and output to physically realistic values in many instances, and minimizes the need for parameter optimization. Example simulations demonstrate that our modeling formulation is qualitatively consistent with observed trends for retention with colloid size and concentration, grain size, and velocity for many systems. The model provides a clear conceptual explanation for the causes of hyperexponential, exponential, uniform, and nonmonotonic retention profiles without invoking hypotheses with regard to colloid heterogeneity, aggregation, or multiple deposition rates. Furthermore, the model formulation and research presented herein helps to identify areas where additional research and theory development are still needed.

1.   Introduction

[2]   Unfavorable attachment conditions occur in many natural environments because most colloids and solid surfaces are negatively charged at the prevailing pH conditions [*Wan and Tokunaga*, 2002]. In this case, colloids may interact with the solid-water interface (SWI) at a separation distance as a result of the summation of repulsive electrostatic and attractive van der Waals interactions, which results in a weak interaction in the secondary minimum, and an energy barrier to attachment in the primary minimum [*Franchi and O'Melia*, 2003; *Hahn et al.*, 2004; *Tufenkji and Elimelech*, 2005a; *Kuznar and Elimelech*, 2007]. Microscopic physical or chemical heterogeneity can also lead to local reductions in the energy barrier height and weak adhesive interactions at a separation distance due to repulsive interactions from neighboring regions [*Elimelech et al.*, 2003; *Hoek and Agarwal*, 2006; *Kozlova and Santore*, 2006, 2007; *Kalasin and Santore*, 2008; *Duffadar and Davis*, 2007, 2008; *Duffadar et al.*, 2009]. Weak adhesive interactions at a separation distance may also occur for colloids under otherwise favorable attachment conditions as a result of forces that are neglected in Derjaguin, Landau, Verwey, and Overbeek (DLVO) theory [*Derjaguin and Landau*, 1941; *Verwey and Overbeek*, 1948], such as electrosteric repulsion, hydration forces, and Born repulsion [*Elimelech et al.*, 1995; *Israelachvili*, 1992].

[3]   There are many important consequences for weak adhesive interactions of colloids with the SWI at a separation distance. First, only a fraction of the colloids that collide with the SWI may interact because a fraction will possess sufficient kinetic energy to overcome the weak adhesive interaction [*Yao et al.*, 1971; *Ryan and Elimelech*, 1996; *Simoni et al.*, 1998; *Dong et al.*, 2002; *Shen et al.*, 2007]. Second, a fraction of the interacting colloids may detach from the SWI due to random variations in kinetic energy (diffusion) [*Simoni et al.*, 1998; *Dong et al.*, 2002; *Shen et al.*, 2007]. Third, the interacting colloids may be susceptible to removal due to hydrodynamic forces during fluid flow that cause colloids to roll on the SWI to regions where the hydrodynamic force is weaker (grain-grain contacts or surface roughness locations) or the adhesive force is stronger (chemical heterogeneity) [*Hubbe*, 1984; *Bergendahl and Grasso*, 1998, 1999, 2000; *Elimelech et al.*, 2003; *Bradford et al.*, 2007, 2011; *Torkzaban et al.*, 2007, 2008]. Fourth, only a fraction of the solid surface area may contribute to colloid immobilization [*Song and Elimelech*, 1994; *Bradford et al.*, 2007, 2011; *Torkzaban et al.*, 2007,

---

[1]US Salinity Laboratory, USDA, ARS, Riverside, California, USA.
[2]Department of Environmental Sciences, University of California, Riverside, California, USA.

2008]. Fifth, this fraction may fill up with time, and the rate of filling will depend on the colloid concentration [*Adamczyk et al.*, 1994; *Song and Elimelech*, 1994; *Kim et al.*, 2009; *Bradford et al.*, 2009a].

[4] Mathematical models have been developed in an attempt to describe colloid transport and retention under unfavorable attachment conditions. The most common models employ the advective dispersion equation with first order colloid attachment and detachment terms [*Harvey and Garabedian*, 1991; *Corapcioglu and Choi*, 1996; *Bolster et al.*, 1999; *Schijven and Hassanizadeh*, 2000]. The attachment coefficient is typically determined using filtration theory [*Yao et al.*, 1971], with a modification to account for the fact that only a fraction of the colliding colloids attach to the SWI [*Ryan and Elimelech*, 1996]; i.e., the so called sticking efficiency α (–). The value of α is frequently considered to be an empirical parameter determined by fitting to experimental data, although theory has also been developed to predict α [*Simoni et al.*, 1998; *Dong et al.*, 2002; *Shen et al.*, 2007]. It should be noted, however, that first-order attachment/detachment models have been unable to account for many experimental observations. This includes the observed colloid transport and retention dependence on solution chemistry, grain size, water velocity, and colloid concentration [*Song and Elimelech*, 1994; *Bradford et al.*, 2003, 2006a, 2006b, 2007; *Tufenkji and Elimelech*, 2005a, 2005b; *Tong et al.*, 2005; *Li and Johnson*, 2005; *Li et al.*, 2005; *Johnson et al.*, 2007; *Torkzaban et al.*, 2007, 2008]. In particular, the shape of the colloid retention profiles (RPs) is frequently not exponential with depth [*Albinger et al.*, 1994; *Baygents et al.*, 1998; *Simoni et al.*, 1998; *Bolster et al.*, 2000; *DeFlaun et al.*, 1997; *Zhang et al.*, 2001; *Redman et al.*, 2001; *Bradford et al.*, 2002, 2006a, 2006b, 2007, 2009a; *Li et al.*, 2004; *Bradford and Bettahar*, 2005, 2006; *Tong et al.*, 2005], in contrast to predictions of first-order attachment models. In an attempt to account for these discrepancies a variety of two-site chemical nonequilibrium [*Schijven et al.*, 2002; *Bradford et al.*, 2003; *Tufenkji and Elimelech*, 2005b], physical nonequilibrium [*Cherrey et al.*, 2003], chemical and physical nonequilibrium [*Leij and Bradford*, 2009], dual permeability [*Bradford et al.*, 2009b; *Yuan and Shapiro*, 2011], and stochastic models [*Bradford and Toride*, 2007; *Shapiro and Bedrikovetsky*, 2010] have been developed. These models have provided an improved description of collected experimental data, but model parameters are largely empirical and obtained by optimization to experimental data. To date, no model exists that provide reliable predictions of colloid transport and retention under unfavorable conditions, even under relatively simple, well defined conditions.

[5] The objective of this work is to present a mathematical model for colloid transport and retention under unfavorable conditions that accounts for observed trends in velocity, adhesive interaction, concentration, and grain size. Our approach considers the five factors described above for weak adhesive interactions. Below we describe the mathematic model, the approach used to estimate model parameters, and provide example simulations to demonstrate the predicted sensitivity to colloid size, grain size, velocity, adhesive interaction, and concentration. We then provide illustrative comparisons to experimental data.

2. Theory

[6] The dual permeability model formulation is quite flexible and has been used to describe hyperexponential [*Bradford et al.*, 2009b] and nonmonotonic [*Yuan and Shapiro*, 2011] RPs in homogeneous porous media. These simulation results suggest that the dual-permeability model provides a promising physical interpretation for colloid retention under unfavorable attachment conditions. Unfortunately, the dual permeability model contains a large number of coupled parameters that have not yet been reliably measured or predicted. Consequently, the dual permeability model has been of limited utility because its parameters have to be fitted to experimental data and the optimization is frequently nonunique. Below we present an improved conceptual and mathematical description of colloid transport and retention in saturated porous media, and provide an initial estimate of the associated dual permeability model parameters. Our approach constrains the model parameters and output to physically realistic values in many instances, and thereby minimizes the need for parameter optimization. In addition, our model framework and theory helps to identify gaps in knowledge and provides a starting point for further model improvement.

2.1. Mass Balance Equations

[7] Colloid transport and retention is conceptualized as shown in Figure 1. Colloids are transported through the bulk aqueous phase by advection and dispersion in region 1. Region 2 is associated with the zone of colloid interaction with the SWI. The thickness of region 2 is very small (on
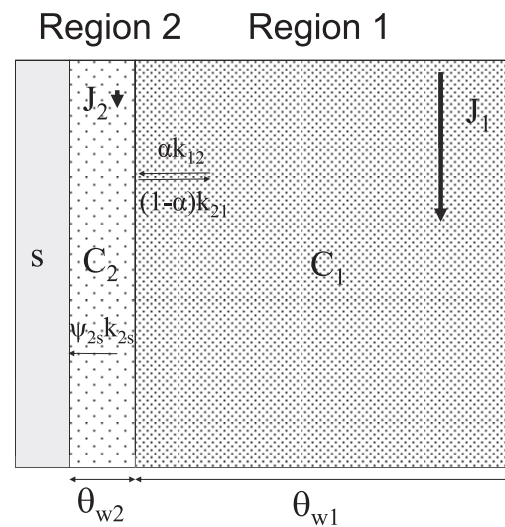
Figure 1. A conceptual picture of the flow and colloid transport processes that are implemented in our model formulation. The subscripts 1 and 2 on parameters denote the respective regions, C is the colloid concentration in the aqueous phase, J is the colloid flux, θ_w is the volumetric water content, s is the colloid concentration on the solid phase, k_{2s} is the first order colloid immobilization rate coefficient from region 2 to the solid phase, k_{12} is the mass transfer coefficient for colloids from region 1 to 2, k_{21} is the mass transfer coefficient for colloids from region 2 to 1, ψ_{2s} accounts for time and concentration dependent blocking, and α is the colloid sticking efficiency.

the order of the colloid size). Colloids may be transported by advection and dispersion in region 2, but the velocity is much lower than in region 1. Mass transfer of colloids to and from regions 1 to 2 is quantified using first-order kinetic expressions. Only a fraction of the colloids in region 2 will interact with the solid phase at any given time, and this fraction is subject to kinetic retention and release. Immobilized colloids on the solid phase may fill up retention locations over time.

[8] The following aqueous and solid phase mass balance equations apply to this conceptual model:

$$\frac{\partial(\theta_{w1}C_1)}{\partial t} = -\frac{\partial J_1}{\partial z} - \theta_{w1}\alpha k_{12}C_1 + \theta_{w2}(1-\alpha)k_{21}C_2, \quad (1)$$

$$\frac{\partial(\theta_{w2}C_2)}{\partial t} = -\frac{\partial J_2}{\partial z} + \theta_{w1}\alpha k_{12}C_1 - \theta_{w2}(1-\alpha)k_{21}C_2 \\ - \theta_{w2}\psi_{2s}k_{2s}C_2, \quad (2)$$

$$\frac{\partial(\rho_b s)}{\partial t} = \theta_{w2}\psi_{2s}k_{2s}C_2, \quad (3)$$

where subscripts 1 and 2 denote the respective regions, t (T; T denotes units of time) is time, z (L; L denotes units of length) is the depth, C (N_c L^{-3}; N_c denotes the number of colloids) is the colloid concentration in the aqueous phase, J (N_c L^{-2} T^{-1}) is the colloid flux (the sum of the advective and dispersive fluxes), θ_w (–) is the volumetric water content, s (N_c M^{-1}; M denotes units of mass) is the colloid concentration on the solid phase, ρ_b (M L^{-3}) is the bulk density, k_{2s} (T^{-1}) is the first order colloid immobilization rate coefficient from region 2 to the solid phase, k_{12} (T^{-1}) is the mass transfer coefficient for colloids from region 1 to 2, and k_{21} (T^{-1}) is the mass transfer coefficient for colloids from region 2 to 1. The parameter ψ_{2s} (–) accounts for time and concentration dependent blocking using a Langmuirian approach as [*Adamczyk*, 1994]:

$$\psi_{2s} = 1 - \frac{s}{s_{\max}}, \quad (4)$$

where $s_{\max}$ (N_c M^{-1}) is the maximum solid phase concentration of retained colloids. The total water flux (q_t; L T^{-1}), volumetric water content (θ_{wt}), and flux concentration of colloids (C_t, N_c L^{-3}) are given in the model as [*Šimůnek and van Genuchten*, 2008]:

$$q_t = q_1 + q_2, \quad (5)$$

$$\theta_{wt} = \theta_{w1} + \theta_{w2}, \quad (6)$$

$$C_t = \frac{q_1 C_1 + q_2 C_2}{q_1 + q_2}, \quad (7)$$

where q_1 and q_2 (L T^{-1}) are the Darcy velocities for regions 1 and 2, respectively.

[9] The model outlined above has been implemented into the COMSOL software package (COMSOL, Inc., Palo Alto, CA 94,301) and into HYDRUS1D [*Šimůnek et al.*, 2008]. The model is coupled with a nonlinear least squares optimization routine based upon the Levenberg-Marquardt

algorithm [*Marquardt*, 1963] to determine model parameters from measured breakthrough curves (BTCs) and/or RPs. For the simulations discussed below, a third-type boundary condition was used at the inlet, and a concentration gradient of zero was fixed at z equal to the outlet depth.

2.2. Determination of Parameters

[10] Our conceptual model (Figure 1) assumes that region 2 is associated with the zone of colloid interaction with the SWI. Consequently, an initial estimate for the value of θ_{w2} was obtained as the product of the geometric solid surface per unit volume (A_s, L^{-1}) and a boundary thickness (L_2, L) that is given as

$$\theta_{w2} = A_s L_2 = A_s(2r_c + h), \quad (8)$$

where r_c (L) is the colloid radius and h (L) is the interaction energy separation distance. The value of h was initially set equal to 20 nm in this work to be consistent with a secondary minimum interaction. The value of θ_{w1} follows directly from equation (6) and the measured value of θ_{wt}.

[11] The value of q_2 can be determined from θ_{w2} and the median velocity in region 2 (v_2, L T^{-1}) which occurs at a distance of $0.5L_2$ from the SWI as

$$q_2 = \theta_{w2}v_2. \quad (9)$$

Bradford et al. [2011] presented pore scale simulations of water flow in sphere packs, and determined the cumulative density function (CDF) of water velocity adjacent to the SWI. This information was further extended by these authors using scaling and interpolation techniques to predict the CDF of v_2 for a range of grain sizes and distributions, water velocities, and colloid sizes. The value of v_2 can be estimated from this information as

$$v_2 = \frac{L_2}{L_V^*}\left(\frac{d_{50}^*}{d_{50}}\right)\left(\frac{q_t}{q_t^*}\right)\left(\frac{\varepsilon^*}{\varepsilon}\right)v_{50}^*, \quad (10)$$

where the superscript * denotes parameters in the reference simulation, L_V^* (L) is the reference simulation voxel length equal to 1.077×10^{-6} m, d_{50} (L) is the median grain diameter, ε (–) is the porosity, and v_{50}^* (L T^{-1}) is the median boundary water velocity in the reference simulation equal to 7.12×10^{-6} m s^{-1}. The values d_{50}^* and q_t^*/ε^* were 100 μm and 2.8×10^{-5} m s^{-1}, respectively. The value of q_1 follows directly from equation (5) and the selected value of q_t. Values of the hydrodynamic dispersion coefficients D_1 and D_2 (L^2 T^{-1}), were set equal to the product of their respective pore water velocity and a constant dispersivity (e.g., 0.1 times the length of the simulation domain).

[12] The rate of colloid mass transfer to the SWI under saturated conditions depends on diffusion, sedimentation, and interception. Colloid filtration theory [*Yao et al.*, 1971] is commonly used to estimate this mass transfer coefficient as

$$k_{12} = \frac{3(1-\theta_w)}{2d_{50}}\eta v_{\text{avg}}. \quad (11)$$

Here v_{avg} (L T^{-1}) is the average pore water velocity and η (–) is the collector efficiency. Correlation equations to predict η as a function of system variables have been

developed from pore scale simulations studying colloid mass transfer to the collector surface in the sphere-in-cell model [*Rajagopalan and Tien*, 1976; *Tufenkji and Elimelech*, 2004]. In this work we employ the correlation of *Tufenkji and Elimelech* [2004].

[13] Values of k_{12} in equations (1) and (2) are multiplied by α because only a fraction of the colloids will interact with the solid surface under unfavorable attachment conditions. Several theoretical approaches have been developed to estimate α [*Simoni et al.*, 1998; *Dong et al.*, 2002; *Shen et al.*, 2007]. The kinetic energy method assumes that the distribution of kinetic energies of diffusing colloids can be described by Maxwell's function [*Chandrasekhar*, 1943], and that DLVO or extended DLVO energy profiles accurately predict the strength of the interaction between colloids and collectors. The value of α is then related to the fraction of diffusing colloid particles that possess kinetic energy less than a given dimensionless (divided by $k_b T_k$, where $k_b = 1.38 \times 10^{-23}$ J K^{-1} is the Boltzmann constant and T_k is the temperature in degree Kevin, K) depth of the interaction energy minimum ($\Phi_{\min}$) as

$$\alpha = \int_0^{\Phi_{\min}} \frac{2\sqrt{\Phi}}{\sqrt{\pi}} \exp(-\Phi) d\Phi, \quad (12)$$

where Φ (–) is a dummy variable of integration. The kinetic energy model implies that a complementary fraction of colloids in region 2, $1 - \alpha$, may diffuse away from the solid surface at any given time and values of k_{21} are therefore multiplied by $(1 - \alpha)$ in equations (1) and (2).

[14] It should be noted that filtration theory assumes that interacting colloids are immobilized instantaneously. In this work, we assume that interacting colloids are mobile and may roll along the solid surface until they encounter a location where the torque balance is favorable for immobilization. The rate of colloid immobilization is given by k_{2s}. Recent experimental information under unfavorable attachment conditions supports the assumption of colloid rolling in region 2 [*Kuznar and Elimelech*, 2007], and colloid immobilization near grain-grain contacts [*Bradford et al.*, 2005, 2006a; *Xu et al.*, 2006; *Li et al.*, 2006; *Yoon et al.*, 2006; *Gaillard et al.*, 2007; *Tong et al.*, 2008] and locations associated with surface roughness [*Choi et al.*, 2007] and/or chemical heterogeneity [*Hoek and Agarwal*, 2006; *Kozlova and Santore*, 2006, 2007; *Kalasin and Santore*, 2008; *Duffadar and Davis*, 2007, 2008; *Duffadar et al.*, 2009]. However, we are unaware of any experimental or theoretical information to directly calculate k_{2s} for the complex geometries found in porous media. In the absence of direct measurements, we initially assume that k_{2s} is inversely related to the time it takes colloids in region 2 to travel to a retention location on the solid surface as

$$k_{2s} = \frac{v_2}{d_{uf}}. \quad (13)$$

Here d_{uf} (L) is the average distance that colloids must travel in region 2 to find a retention location. As d_{uf} approaches 0 the value of k_{2s} becomes large so that colloids in region 2 are almost instantaneously immobilized on the solid phase as assumed in filtration theory. Conversely, colloids are

not instantaneously immobilized on the solid surface when $d_{uf} > 0$ but continue to be transported in region 2 until arriving at a retention location.

[15] The value of d_{uf} may be considered as an empirical optimization parameter or a physical estimate may be given as

$$d_{uf} = \frac{\pi d_{50}(1 - S_f)}{2N_f}. \quad (14)$$

[16] Here S_f (–) is the fraction of the collector surface where the torque balance is favorable for immobilization, and N_f (–) is the number of favorable locations of equal size and distribution on the collector surface. On a smooth, chemically homogeneous collector the value of N_f may reflect the average number of grain-grain contacts. Unless otherwise noted we assume in this work a value of $N_f = 5$ to be consistent with this condition. Alternatively, if surface roughness or chemical heterogeneity is controlling the value of S_f then N_f is given as

$$N_f = \frac{\pi d_{50} S_f}{2 d_f}. \quad (15)$$

Here d_f (L) is equal to the average size of the heterogeneity parallel to the collector surface. If surface molecules are hindering the immobilization of colloids with the solid surface, then it is logical to anticipate that other functional forms for N_f would need to be developed.

[17] *Bradford et al.* [2011] presented a detailed approach to predict the value of S_f based on the balance of applied hydrodynamic (T_{applied}, ML^2 T^{-2}) and resisting adhesive (T_{adhesion}, ML^2 T^{-2}) torques. In summary, the value of S_f on a smooth, chemically homogeneous collector (S_f^*) is given as

$$S_f^* = \frac{1}{2} + \frac{1}{2} \text{erf}\left(\frac{\ln(T_{\text{adhesion}}) - \mu}{\sigma\sqrt{2}}\right), \quad (16)$$

where μ and σ are the mean and variance of the lognormal CDF of T_{applied} determined from results of pore scale simulations and scaling approaches. The value of μ for the lognormal distribution is defined as

$$\mu = \ln(T_{50}). \quad (17)$$

The value of T_{50} (ML^2 T^{-2}) corresponds to the median value of T_{applied} on the SWI. *Bradford et al.* [2011] provide a detailed explanation of how to predict this value for various colloids, porous media, and water flow conditions. In equation (16) the CDF of T_{applied} is evaluated at T_{adhesion} to determine S_f^*. The value of T_{adhesion} may be determined using DLVO and JKR theories [*Derjaguin and Landau*, 1941; *Verwey and Overbeek*, 1948; *Johnson et al.*, 1971] or from a coefficient of rolling friction [*Duffadar and Davis*, 2008]. Details are again given by *Bradford et al.* [2011]. It should be mentioned that S_f^* does not account for the potential influence of surface roughness and/or nanoscale chemical heterogeneity which are expected to produce a minimum value of S_f ($S_f^{\min}$). We therefore determine S_f as

$$S_f = S_f^{\min} + S_f^*. \quad (18)$$

Unless otherwise noted we set the value of $S_f^{\min}$ in this work equal to 0.03 based on experimental data presented by *Bradford et al.* [2009a].

[18] It should be mentioned that the value of $s_{\max}$ in equation (4) is related to S_f as [*Kim et al.*, 2009; *Bradford et al.*, 2009a]

$$s_{\max} = \frac{(1 - \gamma)A_s S_f}{A_c \rho_b}, \tag{19}$$

where A_c (L^2 N^{-1}) is the cross section area per colloid, and γ (–) is the porosity of a monolayer packing of colloids on the solid surface. In this work we assume a value of $\gamma = 0.5$ in all simulations based on information presented by *Johnson and Elimelech* [1995].

[19] Equations (1)–(3) are mathematically equivalent to the conventional first-order attachment/detachment model when $k_{2s} = 0$ and $q_2 = 0$. In this case, the attachment and detachment rate coefficients are equal to αk_{12} and $(1 - \alpha) k_{21}$, respectively. The value of $(1 - \alpha)k_{21}$ has important implications for the shape of the BTCs in this model. When $(1 - \alpha)k_{21}$ is low then concentration tailing occurs after recovery of the unretarded breakthrough curve. However, a low value of detachment cannot account for many experimental observations of colloid retention under unfavorable attachment conditions, such as hyperexponential RPs [*Albinger et al.*, 1994; *Baygents et al.*, 1998; *Simoni et al.*, 1998; *Bolster et al.*, 2000; *DeFlaun et al.*, 1997; *Zhang et al.*, 2001; *Redman et al.*, 2001; *Bradford et al.*, 2002; *Li et al.*, 2004; *Bradford and Bettahar*, 2005]. Conversely, when $(1 - \alpha)k_{21}$ is high then the first-order attachment/detachment model approaches linear equilibrium conditions with a retardation coefficient (R) equal to $1 + \alpha k_{12}/(1 - \alpha)k_{21}$ [*Schijven and Hassanizadeh*, 2000]. As a first approximation we assume in this work that $k_{21} = k_{12}$ and this yields a value of $R = 1 + \alpha/(1 - \alpha)$ that is controlled by chemistry as expected. This assumption is certainly justifiable under highly unfavorable attachment conditions with small α and R close to 1 because $\alpha k_{12} \ll (1 - \alpha)k_{21}$ and is consistent with results reported in the literature [*Gargiulo et al.*, 2007, 2008].

[20] It should be mentioned that the outlined model formulation approaches filtration theory predictions under favorable attachment conditions. In particular, the values of α, S_f, and ψ_{2s} go to 1, $(1 - \alpha)k_{21}$ goes to 0, k_{12} is determined using filtration theory [equation (11)], and k_{2s} becomes very large such that colloids that enter region 2 are instantaneously retained.

3. Results and Discussion

3.1. Predictions

[21] Under unfavorable attachment conditions the model predicts a complex coupling between many physical and chemical factors. Below we present representative simulations to demonstrate the sensitivity of the model output to specific input parameters. The simulation domain length was 0.1 m to be representative of typical packed column studies, the initial concentration in the simulation domain was zero, and the input pulse duration was 3 pore volumes (PV). BTCs are presented herein by plotting the relative effluent concentrations [C_t/C_i; where C_i (N$_c$ L^{-3}) is the input concentration] as a function of PV. RPs are shown on a semilog plot of normalized total concentration in region 2 and on the solid phase [$(\rho_b s + \theta_{wt} C_2)/C_i$] as a function of distance from the inlet.

[22] We first examine the influence of grain size and $\Phi_{\min}$ on colloid transport and retention. Figure 2 presents simulated BTCs (Figures 2a and 2c) and RPs (Figures 2b and 2d) when $r_c = 500$ nm, $q_t = 0.1$ cm min^{-1}, $\theta_{wt} = 0.35$, $C_i = 10^6$ N$_c$ mL^{-1}, and $d_{50} = 50, 100, 250, 500,$ and 1000 μm. The value of $\Phi_{\min} = 0.15$ in Figures 2a and 2b, and $\Phi_{\min} = 0.5$ in Figures 2c and 2d. A systematic trend of increasing colloid retention occurs with decreasing d_{50} for both $\Phi_{\min}$ equal to 0.15 and 0.5. This occurs in part because filtration theory predicts that decreasing d_{50} will increase k_{12} in equation (11). In contrast to the predicted filtration theory, however, the RPs are not always log linear with distance. Smaller values of d_{50} and $\Phi_{\min}$ tend to produce more hyperexponential RPs (a greater amount of retention near the inlet). Hyperexponential RPs have been experimentally observed by many researchers under highly unfavorable attachment conditions [*Albinger et al.*, 1994; *Baygents et al.*, 1998; *Simoni et al.*, 1998; *Bolster et al.*, 2000; *DeFlaun et al.*, 1997; *Zhang et al.*, 2001; *Redman et al.*, 2001; *Bradford et al.*, 2002; *Li et al.*, 2004; *Bradford and Bettahar*, 2005]. In addition, RPs have also been observed to become more hyperexponential with decreasing d_{50} [*Bradford et al.*, 2002, 2003]. The implemented mathematical model provides a clear explanation for these observations as will be discussed below.

[23] Hyperexponential RPs occur because θ_{w2} [equation (8)], v_2 [equation (10)], q_2 [equation (9)], and k_{2s} [see equations (13) and (14)] all increase with decreasing d_{50}. Mass transfer to region 2 is controlled by exchange with region 1 (αk_{12}) and J_2 at the inlet (J_2^*). The value of J_2^* increases with decreasing d_{50} and this leads to a greater amount of colloid retention near the inlet. As J_2^* is depleted by colloid retention with distance, then the mass transfer to region 2 is controlled by exchange with region 1 (αk_{12}). Consequently, the relative importance of J_2^* on colloid retention decreases with increasing $\Phi_{\min}$ [due to its influence on α given by equation (12)] and with distance from the inlet. Consistent with this explanation, *Li et al.* [2004], *Tufenkji and Elimelech* [2005a], and *Bradford et al.* [2007] observed that colloid RPs became less hyperexponential with increasing $\Phi_{\min}$. The above information demonstrates that accounting for the median hydrodynamics [equations (8)–(10)] of colloids near the solid surface provides a viable explanation for the dependence of hyperexponential RPs on d_{50} and $\Phi_{\min}$.

[24] It should be emphasized that hyperexponential RPs are not an experimental artifact of the boundary conditions at the soil surface. This behavior has also been observed to occur at textural interfaces when water flows from a coarser to a finer textured material [*Bradford et al.*, 2005], especially for larger colloids. As discussed above, the model predicts that θ_{w2} and q_2 increases with decreasing d_{50}. Consequently, J_2 at the textural interfaces changes and this difference will increase with the contrast in d_{50}. However, it is presently unclear how concentrations in regions 1 and 2 mix at textural interfaces (e.g., mixing may be complete, partial, or absent). Additional research is warranted on this topic.

[25] Figure 3 presents simulated BTCs and RPs when $d_{50} = 250$ μm, $q_t = 0.1$ cm min^{-1}, $\theta_{wt} = 0.35$, $C_i = 10^6$ N$_c$ mL^{-1},
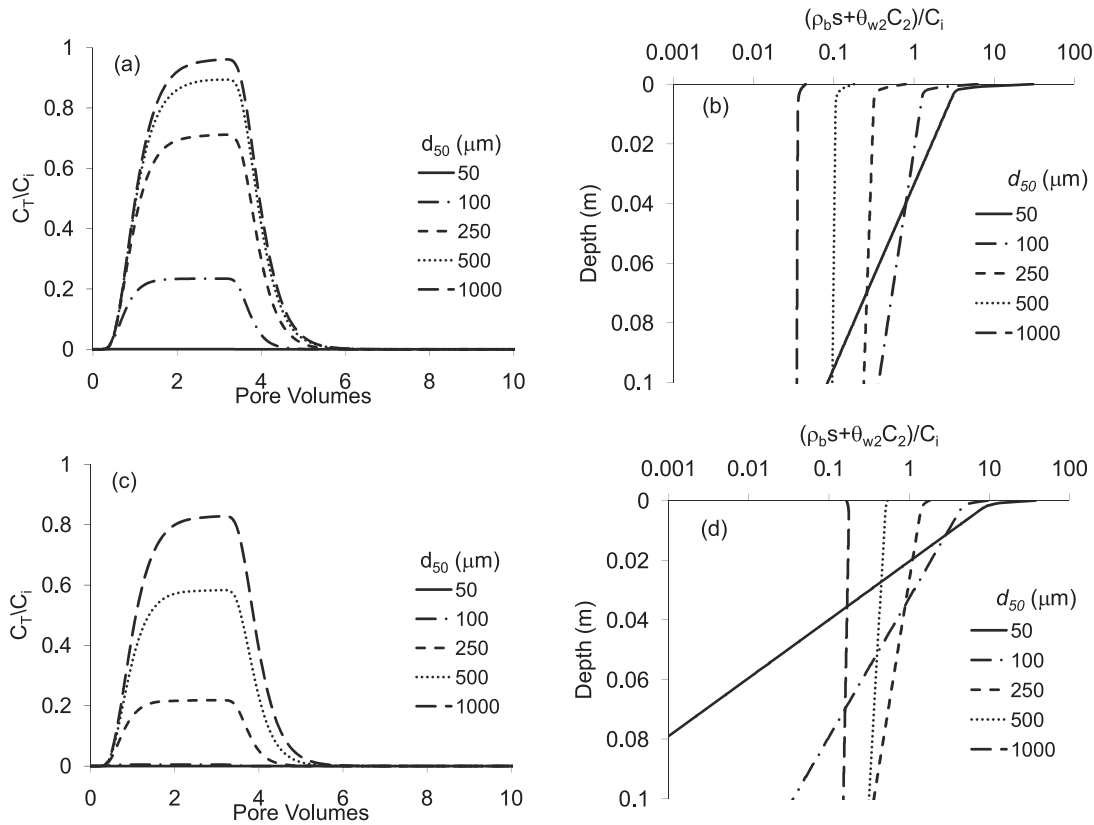
Figure 2. Simulated (a and c) BTCs and (b and d) RPs when $r_c = 500$ nm, $q_t = 0.1$ cm min^{-1}, $\theta_{wt} = 0.35$, $C_i = 10^6$ N$_c$ mL^{-1}, $\Phi_{\min} = $ (a and b) 0.15 and (c and d) 0.5, and $d_{50} = 50, 100, 250, 500$, and 1000 μm. The BTCs are presented herein by plotting the relative effluent concentrations (C_t/C_i) as a function of pore volumes. The RPs are shown on a semilog plot of normalized total concentration in region 2 and on the solid phase [$(\rho_b s + \theta_{wt} C_2)/C_i$] as a function of distance from the inlet.

and $r_c = 250, 500, 1000$, and 2000 nm. Since $\Phi_{\min}$ (the secondary minimum) is also a function of r_c, values of $\Phi_{\min}$ were determined from DLVO calculations assuming a zeta potential of -30 mV for both the colloid and collector, and a ionic strength (IS) of 2 mM of a monovalent electrolyte solution. Under these assumptions the value of $\Phi_{\min}$ was 0.039, 0.079, 0.158, and 0.316 when r_c equals 250, 500, 1000, and 2000 nm, respectively. A systematic increase in colloid retention occurs with increasing r_c. In addition, all of the RPs are hyperexponential and the amount of retention near the inlet increases with r_c (profiles become more hyperexponential). These results are consistent with experimental observations reported in the literature [*Bradford et al.*, 2002, 2003, 2007; *Tufenkji and Elimelech*, 2005a]. It should be mentioned that if Figure 3b was plotted using a nonlog scale then the hyperexponential profiles for the smallest colloids would not have been observable due to their low values. Similarly, the sensitivity of the analytic approach (spectrophotometer or fluorometer) to determine RPs may not always be sufficient to quantify such subtle differences in shape.

[26] A detailed explanation for the observations in Figure 3 can be obtained from the implemented mathematical model. Differences in the amount and shape of the RPs are due to the influence of r_c on J_2^* and on αk_{12}. Values of θ_{w2} [equation (8)], v_2 [equation (10)], q_2 [equation (9)], and k_{2s}

[equation (13)] all increase with increasing r_c. This produces a nonlinear increase in J_2^* with increasing r_c and consequently more hyperexponential RPs. The amount of retention away from the inlet also increases with increasing r_c because of a corresponding increase in k_{2s} and αk_{12} [equations (11) and (12)]. Slight differences in the apparent pulse duration are due to increases in θ_{w2} and corresponding decreases in θ_{w1} with increasing r_c.

[27] Additional simulations were run using the same conditions as in Figure 3, but at a IS = 20 mM (data not shown). Observed trends with r_c were similar to that shown in Figure 3. Similar to differences in Figure 2 with $\Phi_{\min}$, increasing the solution IS produced greater amounts of retention and profiles that are less hyperexponential because the contribution of αk_{12} to retention increases relative to that of J_2^*. It should be mentioned that if a constant value of $\Phi_{\min}$ and α were assumed with r_c in Figure 3 then differences in the retention away from the inlet would have been controlled by k_{12} (instead of αk_{12}). Filtration theory predicts a nonlinear dependence of k_{12} on r_c, with a minimum around $r_c = 1000$ nm. Consequently, a constant value of $\Phi_{\min}$ and α produces a more complex dependence of colloid retention on r_c than that shown Figure 3.

[28] Figure 4 presents simulated BTCs and RPs when $r_c = 500$ nm, $d_{50} = 250$ μm, $q_t = 0.1$ cm min^{-1}, $\theta_{wt} = 0.35$, $\Phi_{\min} = 0.5$, and $C_i = 10^6, 10^7, 10^8, 10^9$, and
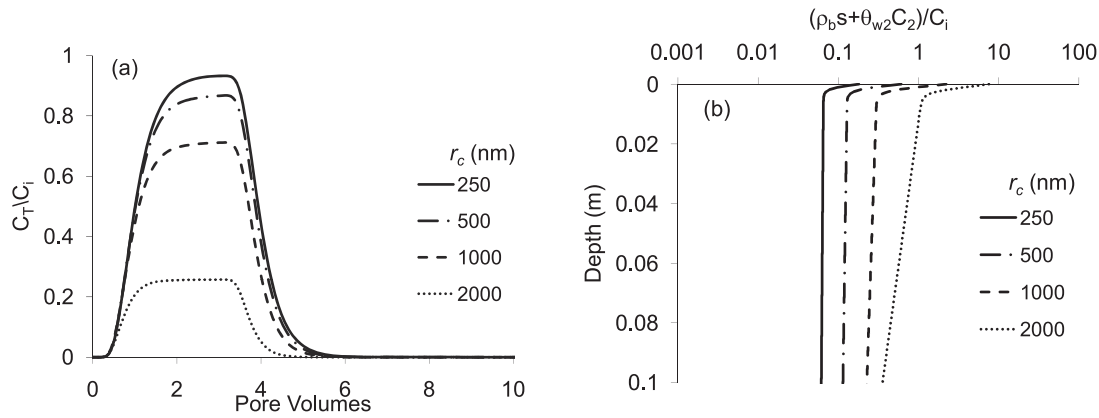
Figure 3. Simulated (a) BTCs and (b) RPs when $d_{50} = 250$ μm, $q_t = 0.1$ cm min^{-1}, $\theta_{wt} = 0.35$, $C_i = 10^6$ N$_c$ mL^{-1}, and $r_c = 250$, 500, 1000, and 2000 nm. Values of Φ_{min} were determined from DLVO calculations when the zeta potential of the colloid and collector were -30 mV and the IS of a monovalent electrolyte solution was 2 mM.

10^{10} N$_c$ mL^{-1}. This data was normalized by C_i so that differences in transport and retention behavior were apparent. Results indicate that above a threshold in C_i (or input pulse duration) the normalized BTCs become sensitive to C_i. In this case, the threshold value is greater than $C_i = 10^8$ N$_c$ mL^{-1}. Values of C_i above this threshold influence the shape of the BTCs and the RPs, with the BTCs exhibiting blocking behavior (a decreasing rate of retention over time) and the RPs transitioning from exponential to uniform in shape with depth. Our mathematical formulation indicates that this occurs as a result of decreases in ψ_{2s} [equations (4) and (19)] with filling of retention sites. Furthermore, the model predicts a sensitivity of colloid transport and retention to C_i that is a function of colloid size, grain size, chemistry, and velocity. For example, similar simulations to those shown in Figure 4 were conducted with $\Phi_{min} = 0.15$ (data not shown). In this case, analogous concentration effects on the BTCs and RPs occurred to those shown in Figure 4 but over a smaller range in retention values because the value of Φ_{min} determines α and therefore the maximum amount of retention. However, when $\Phi_{min} = 0.15$ the RPs transitioned from hyperexponential to uniform in shape with depth as C_i varied from 10^6 to 10^{10} N$_c$ mL^{-1}. Simulated transport and retention trends with C_i are qualitatively consistent with experimental observations reported in the literature [*Tan et al.*, 1994; *Lindqvist et al.*, 1994; *Liu et al.*, 1995; *Bradford and Bettahar*, 2006; *Bradford et al.*, 2009a]. However, additional research is warranted to test the predicted concentration dependency over a wider range of experimental conditions and to improve the conceptual modeling framework. For example, we postulate that the value of α may decrease with higher values of C_i because the number of colloid collisions increases with C_i and the kinetic energy distribution may therefore not be accurately described by the Maxwellian distribution [*Chapman and Cowling*, 1991; *Bradford and Bettahar*, 2006].

[29] Figure 5 presents simulated BTCs and RPs when $r_c = 500$ nm, $d_{50} = 250$ μm, $\theta_{wt} = 0.35$, $\Phi_{min} = 0.15$, $C_i = 10^6$ N$_c$ mL^{-1}, and q_t equals 0.01, 0.05, 0.1, 0.2, and 0.4 cm min^{-1}. A systematic decrease in colloid retention occurs with increasing q_t. This result is consistent with experimental observations reported in the literature [*Kretzschmar and Sticher*, 1998; *Schijven and Hassanizadeh*, 2000]. Filtration theory predicts that k_{12} is approximately proportional to v_{avg} raised to the 1/3 power [*Schijven and Hassanizadeh*, 2000]. However, the overall rate of advection is proportional to v_{avg}. Consequently, filtration theory predicts that colloid retention will decrease with increasing v_{avg}.
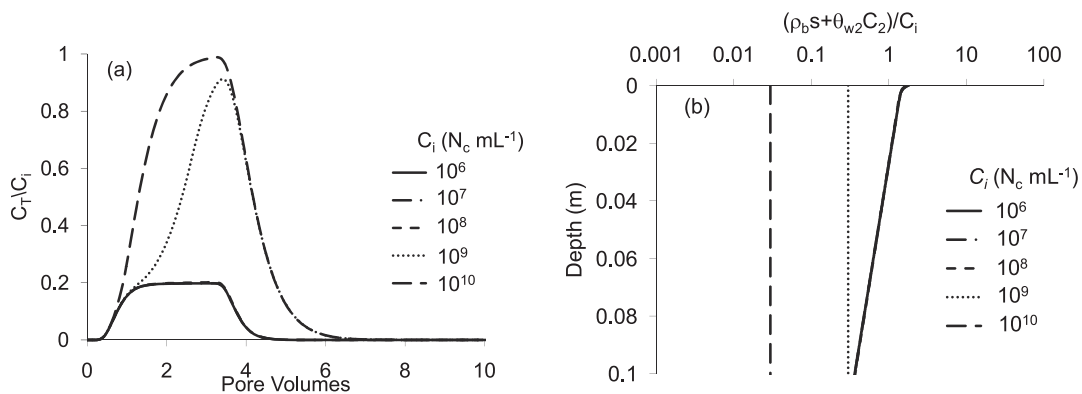

Figure 4. Simulated (a) BTCs and (b) RPs when $r_c = 500$ nm, $d_{50} = 250$ μm, $q_t = 0.1$ cm min^{-1}, $\theta_{wt} = 0.35$, $\Phi_{min} = 0.5$, and $C_i = 10^6$, 10^7, 10^8, 10^9, and 10^{10} N$_c$ mL^{-1}.
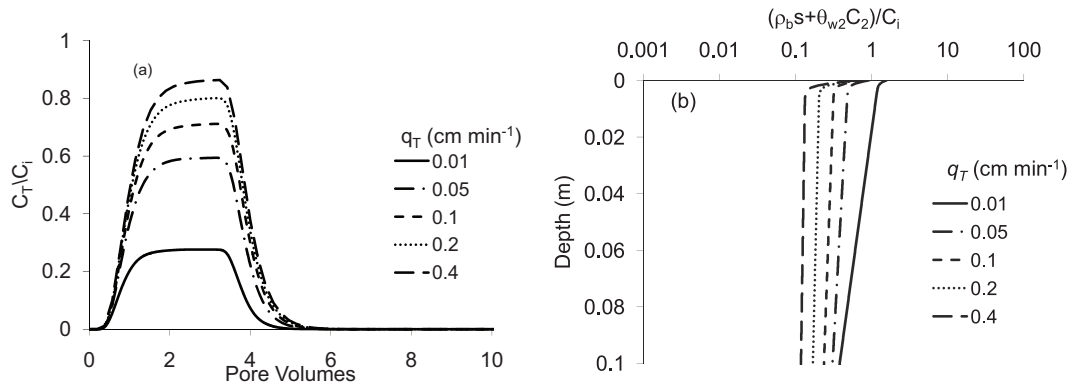
Figure 5. Simulated (a) BTCs and (b) RPs when $r_c = 500$ nm, $d_{50} = 250$ μm, $\theta_{wt} = 0.35$, $\Phi_{min} = 0.15$, $C_i = 10^6$ N$_c$ mL^{-1}, and q_t equals 0.01, 0.05, 0.1, 0.2, and 0.4 cm min^{-1}.

[30] The retention profile in Figure 5b is almost exponential at the lowest value of $q_t = 0.01$ cm min^{-1}, but becomes increasingly hyperexponential for increasing q_t. Values of v_2, q_2, and (in these simulations) k_{2s} increase with increasing q_t. This produces an increase in J_2^* with increasing q_t and consequently more hyperexponential RPs. This predicted trend has not yet been experimentally verified. In fact, *Li et al.* [2004] and *Bradford et al.* [2007] reported that RPs became less hyperexponential with increasing velocity. This discrepancy could arise from a velocity dependency on α [*Johnson et al.*, 2007] that is not accounted for in equation (12), analytical insensitivity to lower concentrations of retained colloids, or the dependency of RPs on C_i as previously demonstrated. In addition, the simulated value of S_f was not influenced much by changes in q_t for the considered Φ_{min} and r_c. However, variations in Φ_{min} and r_c over a wider range of conditions is expected to influence S_f [*Torkzaban et al.*, 2007; *Bradford et al.*, 2011] and a decreasing value of S_f with q_t would increase the sensitivity of RPs to C_i. Additional research is warranted on all of these velocity related topics. It should be mentioned that similar simulations to those shown in Figure 5 were conducted using $\Phi_{min} = 0.5$ (data not shown). Similar to Figure 2, increasing Φ_{min} to 0.5 produced a greater amount of retention and profiles that were less hyperexponential than those shown in Figure 5. However, overall trends of decreasing retention with increasing q_t were preserved.

3.2. Analysis of Experimental Data

[31] The outlined model was used to describe transport and retention data for monodispersed suspensions of fluorescent 1 μm carboxyl latex microspheres [*Bradford and Bettahar*, 2006; *Bradford et al.*, 2007, 2009a] and *E. coli* O157:H7/pGFP [*Bradford et al.*, 2006b] in saturated, pack column experiments under unfavorable attachment conditions. The selected data for analysis exhibits a wide range of transport and retention behavior that is intended to illustrate the capabilities and limitations of this model.

[32] Experimental details are given in the indicated publications, but will be briefly highlighted below. Selected sieve sizes of sand were wet packed into 4.8 cm diameter by 15 cm long columns that were equipped with an adjustable length flow adapter. A salt cleaning method [*Bradford*

et al., 2002] was used to remove trace amounts of clay from the packed sand. An electrolyte solution with a selected chemistry was prepared for the resident, tracer, and eluting solutions. The sand in the columns was equilibrated with the resident solution, and then a tracer solution of microspheres or *E. coli* O157:H7 was pumped through the packed columns at a steady flow rate for several PV followed by continued flushing with the eluting solution. The sand in the columns was incrementally excavated into vials containing excess eluting solution, the vials were shaken, an aliquot was collected for analysis, and the mass of sand in the vials was determined after drying. The concentrations of fluorescent microspheres or *E. coli* O157:H7 were determined in the solution from the column effluent and vials using a fluorometer. A mass balance was conducted based on measured concentrations in the influent, effluent, and sand.

[33] Figure 6 presents observed and simulated BTCs and RPs for carboxyl latex microspheres under several different conditions of solution chemistry (curves 1, 2, and 3 were for pH = 7 and IS = 1 mM, pH = 10 and IS = 31 mM, and pH = 10 and IS = 81 mM, respectively), colloid hydrophobicity (curves 1, 2, and 3 were hydrophobic, hydrophilic, and hydrophilic, respectively), and C_i (curves 1, 2, and 3 were for 3.9×10^7, 3.9×10^9, and 2.7×10^7 N$_c$ mL^{-1}, respectively), but for similar values of $r_c = 500$ nm, $d_{50} = 150$ μm, $q_t = 0.1$ cm min^{-1}, $\theta_{wt} = 0.35$, and pulse duration (1.5–2.1 PV). Curves 1, 2, and 3 approached hyperexponential, uniform, and exponential distributions with depth. The simulations were obtained by optimizing values of α and L_2 to the curves, and the dispersivities were set equal to 0.01 cm be consistent with the data. The coefficient of linear regression (r^2) between observed and simulated data ranged from 0.85 to 0.94, and this indicates that the optimized model gave a reasonable description to a wide range of experimental data and retention profile shapes. It should be mentioned that the time dependent retention behavior observed in curves 1 and 2 was incompletely characterized by the model because values of s_{max} were predicted instead of optimized.

[34] Optimized values of α to curves 1, 2, and 3 were equal to 0.025, 0.045, and 0.055, respectively. These values of α account for differences in solution chemistry and colloid hydrophobicity, and increased with IS due to compression of the double layer thickness and a corresponding
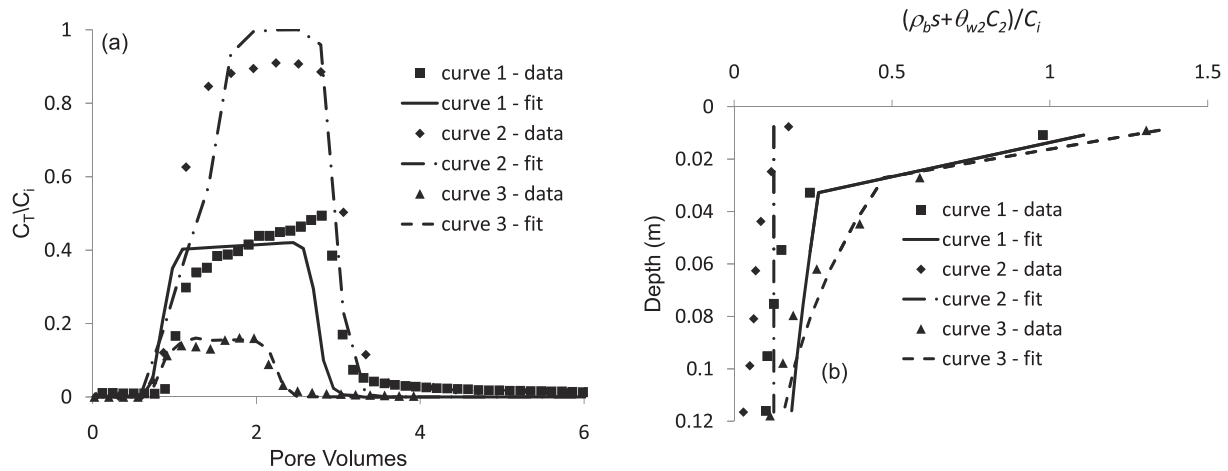
Figure 6. Observed and simulated (a) BTCs and (b) RPs for carboxyl latex microspheres under several different conditions of solution chemistry (curves 1, 2, and 3 were for pH = 7 and IS = 1 mM, pH = 10 and IS = 31 mM, and pH = 10 and IS = 81 mM, respectively), colloid hydrophobicity (curves 1, 2, and 3 were hydrophobic, hydrophilic, and hydrophilic, respectively), and C_i (curves 1, 2, and 3 were for 3.9×10^7, 3.9×10^9, and 2.7×10^7 N_c mL^{-1}, respectively), but for similar values of $r_c = 500$ nm, $d_{50} = 150$ μm, $q_t = 0.1$ cm min^{-1}, $\theta_{wt} = 0.35$, and pulse durations (1.5–2.1 PV). Values of α were optimized to each data set [*Bradford and Bettahar*, 2006; *Bradford et al.*, 2007, 2009a], as well as a single value of L_2.

increase in the depth of the secondary minimum. To improve the description of the RPs it was also necessary to optimize a single value of $L_2 = 4$ μm. The value of L_2 influences J_2^* by changing θ_{w2}, v_2, and q_2 that were based on information from pore scale water flow simulations on smooth, spherical collector surfaces. Differences in predicted values of L_2 are therefore likely with grain roughness, angularity, and size distribution.

[35] In addition, our modeling approach is based on a number of assumptions with regard to the chemical interaction that may be violated in some instances. For example, our model predictions assumed that the colloid was much larger than any physical or chemical heterogeneity on the colloid and/or collector surface, such that colloids on the collector surface experienced an effective secondary minimum interaction. It should be noted that DLVO theory will not be adequate to characterize the interaction energy when the size of the colloid approaches that of the heterogeneity on the collector surface or when surface macromolecules produce significant non-DLVO forces, and this will lead to corresponding errors in predictions for α, S_f, s_{max}, k_{2s}, and k_{21}. To overcome these limitations additional model assumptions, theory, and/or parameter optimization are required. An illustrative example is given below.

[36] Some bacteria species have been reported in the literature to exhibit nonmonotonic RPs with depth [*Tong et al.*, 2005; *Bradford et al.*, 2006b]. Observed and simulated BTCs and nonmonotonic RPs for *E. coli* O157:H7 are shown in Figure 7 in several different pore volumes (times). Simulations employed values of $r_c = 250$ nm, $d_{50} = 150$ μm, $q_t = 0.1$ cm min^{-1}, $\theta_{wt} = 0.34$, $C_i = 1.72 \times 10^8$ N_c mL^{-1}, and a pulse duration of 75 min that were based on measurements. The values of $\alpha = 0.05$, $S_f = 0.007$, $D_2 = 0.01 \times D_1$, $k_{21} = 0$, and $N_f = 0.01$ had to be optimized by trial and error because of the coupling between parameters and nonuniqueness in the fit. The simulation for *E. coli* O157:H7 clearly

demonstrates that our modeling framework is capable of producing nonmonotonic RPs ($r^2 = 0.76$). Furthermore, predictions for *E. coli* O157:H7 based on these fitted parameter values were able to accurately capture the general transport and retention behavior in several different sands at different velocities [*Bradford et al.*, 2006b] (data not shown), and a slowly moving and spreading nonmonotonic retention profile with time [*Tong et al.*, 2005].

[37] In these simulations we assumed a value of $r_c = 250$ nm based on the width of the rod shaped cells, because they will likely orient horizontally on the SWI. The value of $D_2 = 0.01 \times D_1$ is consistent with the much lower velocities of rod shaped cells next to the SWI than in region 1. Values of k_{21} and N_f were much lower than those predicted previously, which suggests hindered cell release and immobilization by surface macromolecules. Additional research is needed to predict all of these fitted parameters over a wide range of conditions.

4. Summary and Conclusions

[38] A mathematical modeling formulation was presented to describe colloid transport in saturated porous media under unfavorable attachment conditions. The model accounts for colloid transport in the bulk aqueous phase and adjacent to the solid phase, and rates of colloid collision, interaction, release, and immobilization on the solid phase. Colloid immobilization depends on all these factors. However, the relative importance of a given process can change with transport distance and filling of retention locations. The exact location and mechanism of retention is not explicitly considered in this work, just the rate of immobilization which depends on the velocity adjacent to the solid phase and the amount and distribution of retention locations (e.g., grain-grain contacts, surface roughness, and chemical heterogeneity).
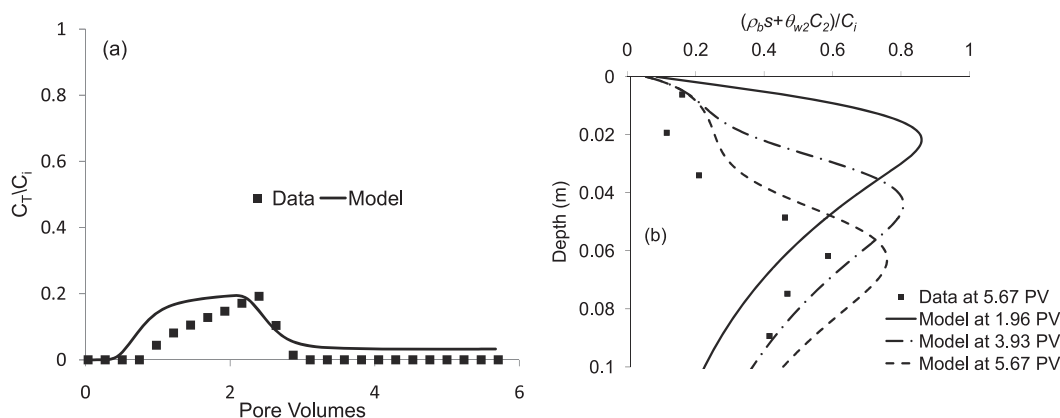
Figure 7. Observed and simulated (a) BTCs and (b) RPs for *E. coli* O157:H7. The value of $r_c = 250$ nm, $d_{50} = 150$ μm, $q_t = 0.1$ cm min^{-1} and $\theta_{wt} = 0.35$ were based on measurements. The values of $\alpha = 0.05$, $S_f = 0.007$, $D_2 = 0.01^*D_1$, $k_{21} = 0$, and $k_{2s} = 0.01$ min^{-1} were optimized to the *E. coli* O157:H7 data [*Bradford et al.*, 2006b].

[39] Simulations presented herein indicate that our modeling formulation is at least qualitatively consistent with observed trends for retention with d_{50}, r_c, C_i, and q_t for many systems. Furthermore, the model provides a clear conceptual explanation for the causes of hyperexponential, exponential, uniform, and nonmonotonic RPs without invoking hypotheses with regard to colloid heterogeneity, aggregation, or multiple deposition rates. Hyperexponential RPs occur when J_2^* is larger than the net colloid exchange rate from the bulk aqueous phase to the solid surface. This effect increases for large colloid sizes, smaller grain sizes, and higher velocities under highly unfavorable attachment conditions. In contrast, exponential RPs occur when the net colloid exchange rate from the bulk aqueous phase to the solid surface dominates such as for smaller colloid sizes, larger grain sizes, lower velocities, and conditions that are more favorable for attachment. Uniform RPs occur when small amounts of retention sites are filled at higher input concentration and/or longer pulse durations. Nonmonotonic profiles reflect an increase in the residence time of mobile colloids on the solid phase due to a decrease in the rates of release and immobilization, presumably due to surface macromolecules.

[40] The research presented herein also helps to identify areas where additional studies are needed. For example, what are the implications of J_2 at textural interfaces and in heterogeneous soils under conditions that produce hyperexponential RPs? Is the value of α also a function of velocity and concentration? How do we account for transients in solution chemistry in the above model formulation? How do we predict model parameters when DLVO theory is not valid and on rough surfaces?

References

Adamczyk, Z., B. Siwek, M. Zembala, and P. Belouschek (1994), Kinetics of localized adsorption of colloid particles, *Adv. Colloid Interface Sci.*, *48*, 151–280.

Albinger, O., B. K. Biesemeyer, R. G. Arnold, and B. E. Logan (1994), Effect of bacterial heterogeneity on adhesion to uniform collectors by monoclonal populations, *FEMS Microbiol. Lett.*, *124*(3), 321–326.

Baygents, J. C., J. R. Glynn Jr., O. Albinger, B. K. Biesemeyer, K. L. Ogden, and R. G. Arnold (1998), Variation of surface charge density in monoclonal bacterial populations: Implications for transport through porous media, *Environ. Sci. Technol.*, *32*, 1596–1603.

Bergendahl, J., and D. Grasso (1998), Colloid generation during batch leaching tests: Mechanics of disaggregation, *Colloid Surf. A: Physicochem. Eng. Aspects*, *135*, 193–205.

Bergendahl, J., and D. Grasso (1999), Prediction of colloid detachment in a model porous media: Thermodynamics, *AIChE J.*, *45*, 475–484.

Bergendahl, J., and D. Grasso (2000), Prediction of colloid detachment in a model porous media: Hydrodynamics, *Chem. Eng. Sci.*, *55*, 1523–1532.

Bolster, C. H., A. L. Mills, G. M. Hornberger, and J. S. Herman (1999), Spatial distribution of deposited bacteria following miscible displacement experiments in intact cores, *Water Resour. Res.*, *35*, 1797–1807, doi:10.1029/1999WR900031.

Bolster, C. H., A. L. Mills, G. Hornberger, and J. Herman (2000), Effect of intra-population variability on the long-distance transport of bacteria, *Ground Water*, *38*(3), 370–375.

Bradford, S. A., and M. Bettahar (2005), Straining, attachment, and detachment of *Cryptosporidium* oocysts in saturated porous media, *J. Environ. Qual.*, *34*, 469–478.

Bradford, S. A., and M. Bettahar (2006), Concentration dependent colloid transport in saturated porous media, *J. Contamin. Hydrol.*, *82*, 99–117.

Bradford, S. A., and N. Toride (2007), A stochastic model for colloid transport and deposition, *J. Environ. Qual.*, *36*, 1346–1356.

Bradford, S. A., S. R. Yates, M. Bettahar, and J. Šimůnek (2002), Physical factors affecting the transport and fate of colloids in saturated porous media, *Water Resour. Res.*, *38*, 1327(12), doi:10.1029/2002WR001340.

Bradford, S. A., J. Šimůnek, M. Bettahar, M. Th. van Genuchten, and S. R. Yates (2003), Modeling colloid attachment, straining, and exclusion in saturated porous media, *Environ. Sci. Technol.*, *37*, 2242–2250.

Bradford, S. A., J. Šimůnek, M. Bettahar, Y. F. Tadassa, M. Th. van Genuchten, and S. R. Yates (2005), Straining of colloids at textural interfaces, *Water Resour. Res.*, *41*, W10404, doi:10.1029/2004WR003675.

Bradford, S. A., J. Šimůnek, M. Bettahar, M. Th. van Genuchten, and S. R. Yates (2006a), Significance of straining in colloid deposition: Evidence and implications, *Water Resour. Res.*, *42*, W12S15, doi:10.1029/2005WR004791.

Bradford, S. A., J. Šimůnek, and S. L. Walker (2006b), Transport and straining of *E. coli* O157:H7 in saturated porous media, *Water Resour. Res.*, *42*, W12S12, doi:10.1029/2005WR004805.

Bradford, S. A., S. Torkzaban, and S. L. Walker (2007), Coupling of physical and chemical mechanisms of colloid straining in saturated porous media, *Water Res.*, *41*, 3012–3024.

Bradford, S. A., H. N. Kim, B. Z. Haznedaroglu, S. Torkzaban, and S. L. Walker (2009a), Coupled factors influencing concentration dependent colloid transport and retention in saturated porous media, *Environ. Sci. Technol.*, *43*, 6996–7002.

Bradford, S. A., S. Torkzaban, F. Leij, J. Šimůnek, and M. Th. van Genuchten (2009b), Modeling the coupled effects of pore space geometry and velocity on colloid transport and retention, *Water Resour. Res.*, *45*, W02414, doi:10.1029/2008WR007096.

Bradford, S. A., S. Torkzaban, and A. Wiegmann (2011), Pore-scale simulations to determine the applied hydrodynamic torque and colloid immobilization, *Vadose Zone J.*, *10*, 252–261.

Chandrasekhar, S. (1943), Stochastic problems in physics and astronomy, *Rev. Mod. Phys.*, *15*, 1–89.

Chapman, S., and T. G. Cowling (1991), *The Mathematical Theory of Nonuniform Gases*, Cambridge University Press, Cambridge, UK, p. 447.

Cherrey, K. D., M. Flury, and J. B. Harsh (2003), Nitrate and colloid transport through coarse Hanford sediments under steady state, variably saturated flow, *Water Resour. Res.*, *39*(6), 1165, doi:10.1029/2002WR001944.

Choi, N. C., D. J. Kim, and S. B. Kim (2007), Quantification of bacterial mass recovery as a function of pore-water velocity and ionic strength, *Res. Microbiol.*, *158*, 70–78.

Corapcioglu, M. Y., and H. Choi (1996), Modeling colloid transport in unsaturated porous media and validation with laboratory column data, *Water Resour. Res.*, *32*, 3437–3449, doi:10.1029/95WR02693.

DeFlaun, M. F., C. J. Murray, M. Holben, T. Scheibe, A. Mills, T. Ginn, T. Griffin, E. Majer, and J. L. Wilson (1997), Preliminary observations on bacterial transport in a coastal plain aquifer, *FEMS Microbiol. Rev.*, *20*(3–4), 473–487.

Derjaguin, B. V., and L. D. Landau (1941), Theory of the stability of strongly charged lyophobic sols and of the adhesion of strongly charged particles in solutions of electrolytes, *Acta Physicochim. USSR*, *14*, 733–762.

Dong, H., T. C. Onstott, C.-H. Ko, A. D. Hollingsworth, D. G. Brown, and B. J. Mailloux (2002), Theoretical prediction of collision efficiency between adhesion-deficient bacteria and sediment grain surface, *Colloid Surf. B: Biointerfaces*, *24*, 229–245.

Duffadar, R. D., and J. M. Davis (2007), Interaction of micrometer-scale particles with nanotextured surfaces in shear flow, *J. Colloid Interface Sci.*, *308*, 20–29.

Duffadar, R. D., and J. M. Davis (2008), Dynamic adhesion behavior of micrometer-scale particles flowing over patchy surfaces with nanoscale electrostatic heterogeneity, *J. Colloid Interface Sci.*, *326*, 18–27.

Duffadar, R. D., S. Kalasin, J. M. Davis, and M. M. Santore (2009), The impact of nanoscale chemical features on micron-scale adhesion: Crossover from heterogeneity-dominated to mean field behavior, *J. Colloid Interface Sci.*, *337*, 396–407.

Elimelech, M., J. Gregory, X. Jia, and R. A. Williams (1995), in *Particle Deposition & Aggregation Measurement, Modeling and Simulation*, Butterworth-Heinemann, Woburn, MA.

Elimelech, M., J. Y. Chen, and Z. A. Kuznar (2003), Particle deposition onto solid surfaces with micropatterned charge heterogeneity: The "hydrodynamic bump" effect, *Langmuir*, *19*, 6594–6597.

Franchi, A., and C. R. O'Melia (2003), Effects of natural organic matter and solution chemistry on the deposition and reentrainment of colloids in porous media, *Environ. Sci. Technol.*, *37*(6), 1122–1129.

Gaillard, J. F., C. Chen, S. H. Stonedahl, B. L. T. Lau, D. T. Keane, and A. I. Packman (2007), Imaging of colloidal deposits in granular porous media by X-ray difference micro-tomography, *Geophys. Res. Lett.*, *34*, L18404, doi:10.1029/2007GL030514.

Gargiulo, G., S. A. Bradford, J. Simunek, P. Ustohal, H. Vereecken, and E. Klumpp (2007), Bacteria transport and deposition under unsaturated conditions: The role of the matrix grain size and the bacteria surface protein, *J. Contam. Hydrol.*, *92*, 255–273.

Gargiulo, G., S. A. Bradford, J. Simunek, P. Ustohal, H. Vereecken, and E. Klumpp (2008), Bacteria transport and deposition under unsaturated flow conditions: The role of water content and bacteria surface hydrophobicity, *Vadose Zone J.*, *7*, 406–419.

Hahn, M. W., D. Abadzic, and C. R. O'Melia (2004), Aquasols: On the role of secondary minima, *Environ. Sci. Technol.*, *38*, 5915–5924.

Harvey, R. W., and S. P. Garabedian (1991), Use of colloid filtration theory in modeling movement of bacteria through a contaminated sandy aquifer, *Environ. Sci. Technol.*, *25*, 178–185.

Hoek, E. M. V., and G. K. Agarwal (2006), Extended DLVO interactions between spherical particles and rough surfaces, *J. Colloid Interface Sci.*, *298*, 50–58.

Hubbe, M. A. (1984), Theory of detachment of colloidal particles from plat surfaces exposed to flow, *Colloid Surf.*, *12*, 151–178.

Israelachvili, J. N. (1992), in *Intermolecular and Surface Forces*, 2nd ed., Academic, London.

Johnson, K. L., K. Kendall, and A. D. Roberts (1971), Surface energy and the contact of elastic solids, *Proc. R. Soc. London Ser. A*, *11*, 301–313.

Johnson, P. R., and M. Elimelech (1995), Dynamics of colloid deposition in porous media: blocking based on random sequential adsorption, *Langmuir*, *11*, 801–812.

Johnson, W. P., X. Li, and S. Assemi (2007), Deposition and re-entrainment dynamics of microbes and non-biological colloids during non-perturbed transport in porous media in the presence of an energy barrier to deposition, *Adv. Water Resour.*, *30*, 1432–1454.

Kalasin, S., and M. M. Santore (2008), Hydrodynamic crossover in dynamic microparticle adhesion on surfaces of controlled nanoscale heterogeneity, *Langmuir*, *24*, 4435–4438.

Kim, H. N., S. A. Bradford, and S. L. Walker (2009), *Escherichia coli* O157:H7 transport in saturated porous media: Role of solution chemistry and surface macromolecules, *Environ. Sci. Technol.*, *43*(12), 4340–4347.

Kozlova, N., and M. M. Santore (2006), Micron-scale adhesion dynamics mediated by nanometer-scale surface features, *Langmuir*, *22*, 1135–1142.

Kozlova, N., and M. M. Santore (2007), Micrometer scale adhesion on nanometer-scale patchy surfaces: Adhesion rates, adhesion thresholds, and curvature-based selectivity, *Langmuir*, *23*, 4782–4791.

Kretzschmar, R., and H. Sticher (1998), Colloid transport in natural porous media: Influence of surface chemistry and flow velocity, *Phys. Chem. Earth*, *23*, 133–139.

Kuznar, Z. A., and M. Elimelech (2007), Direct microscopic observation of particle deposition in porous media: Role of the secondary energy minimum, *Colloid Surf. A: Physicochem. Eng. Aspects*, *294*, 156–162.

Leij, F. J., and S. A. Bradford (2009), Combined physical and chemical nonequilibrium transport model: Analytical solution, moments, and application to colloids, *J. Contam. Hydrol.*, *110*, 87–99.

Li, X., and W. P. Johnson (2005), Non-monotonic variations in removal rate coefficients of microspheres in porous media under unfavorable deposition conditions, *Environ. Sci. Technol.*, *39*, 1658–1665.

Li, X., T. D. Scheibe, and W. P. Johnson (2004), Apparent decreases in colloid deposition rate coefficient with distance of transport under unfavorable deposition conditions: A general phenomenon, *Environ. Sci. Technol.*, *38*, 5616–5625.

Li, X., P. Zhang, C. L. Lin, and W. P. Johnson (2005), Role of hydrodynamic drag on microsphere deposition and re-entrainment in porous media under unfavorable conditions, *Environ. Sci. Technol.*, *39*, 4012–4020.

Li, X., C.-L. Lin, J. D. Miller, and W. P. Johnson (2006), Pore-scale observation of microsphere deposition at grain-to-grain contacts over assemblage-scale porous media domains using X-ray microtomography, *Environ. Sci. Technol.*, *40*, 3762–3768.

Lindqvist, R., J. S. Cho, and C. G. Enfield (1994), A kinetic model for cell density dependent bacterial transport in porous media, *Water Resour. Res.*, *30*, 3291–3299, doi:10.1029/94WR01725.

Liu, D., P. R. Johnson, and M. Elimelech (1995), Colloid deposition dynamics in flow-through porous media: role of electrolyte concentration, *Environ. Sci. Technol.*, *29*, 2963–2973.

Marquardt, D. W. (1963), An algorithm for least squares estimation of nonlinear parameters, *SIAM J.*, *11*, 431–441.

Rajagopalan, R., and C. Tien (1976), Trajectory analysis of deep-bed filtration with the Sphere-in-Cell porous-media model, *AIChE J.*, *22*, 523–533.

Redman, J. A., S. B. Grant, T. M. Olson, and M. K. Estes (2001), Pathogen filtration, heterogeneity, and the potable reuse of wastewater, *Environ. Sci. Technol.*, *35*, 1798–1805.

Ryan, J. N., and M. Elimelech (1996), Colloid mobilization and transport in groundwater, *Colloid Surf. A: Physicochem. Eng. Aspects*, *107*, 1–56.

Schijven, J. F., and S. M. Hassanizadeh (2000), Removal of viruses by soil passage: Overview of modeling, processes, and parameters, *Crit. Rev. Environ. Sci. Technol.*, *30*, 49–127.

Schijven, J. F., S. M. Hassanizadeh, and H. de Bruin (2002), Two-site kinetic modeling of bacteriophages transport through columns of saturated dune sand, *J. Contam. Hydrol.*, *57*, 259–279.

Shapiro, A. A., and P. G. Bedrikovetsky (2010), A stochastic theory for deep bed filtration accounting for dispersion and size distributions, *Physica A*, *389*, 2473–2494.

Shen, C., B. Li, Y. Huang, and Y. Jin (2007), Kinetics of coupled primary- and secondary-minimum deposition of colloids under unfavorable chemical conditions, *Environ. Sci. Technol.*, *41*, 6976–6982.

Simoni, S. F., H. Harms, T. N. P. Bosma, and A. J. B. Zehnder (1998), Population heterogeneity affects transport of bacteria through sand columns at low flow rates, *Environ. Sci. Technol.*, *32*, 2100–2105.

Šimůnek, J., and M. Th. van Genuchten (2008), Modeling nonequilibrium flow and transport using HYDRUS, *Vadose Zone J.*, *7*, 782–797.

Šimůnek, J., M. Th. van Genuchten, and M. Šejna (2008), The HYDRUS-1D software package for simulating the one-dimensional movement of water, heat, and multiple solutes in variably saturated media, Version 4.0, HYDRUS Software Series 3, Department of Environmental Sciences, University of California Riverside, Riverside, CA, p. 315.

Song, L., and M. Elimelech (1994), Transient deposition of colloidal particles in heterogeneous porous media, *J. Colloid Interface Sci.*, *167*, 301–313.

Tan, Y., J. T. Gannon, P. Baveye, and M. Alexander (1994), Transport of bacteria in an aquifer sand: Experiments and model simulations, *Water Resour. Res.*, *30*, 3243–3252, doi:10.1029/94WR02032.

Tong, M., X. Li, C. N. Brow, and W. P. Johnson (2005), Detachment-influenced transport of an adhension-deficient bacterial strain within water-reactive porous media, *Environ. Sci. Technol.*, *39*, 2500–2508.

Tong, M., H. Ma, and W. P. Johnson (2008), Funneling of flow into grain-to-grain contacts drives colloid-colloid aggregation in the presence of an energy barrier, *Environ. Sci. Technol.*, *42*, 2826–2832.

Torkzaban, S., S. A. Bradford, and S. L. Walker (2007), Resolving the coupled effects of hydrodynamics and DLVO forces on colloid attachment to porous media, *Langmuir*, *23*, 9652–9660.

Torkzaban, S., S. S. Tazehkand, S. L. Walker, and S. A. Bradford (2008), Transport and fate of bacteria in porous media: Coupled effects of chemical conditions and pore space geometry, *Water Resour. Res.*, *44*, W04403, doi:10.1029/2007WR006541.

Tufenkji, N., and M. Elimelech (2004), Correlation equation for predicting single-collector efficiency in physiochemical filtration in saturated porous media, *Environ. Sci. Technol.*, *38*, 529–536.

Tufenkji, N., and M. Elimelech (2005a), Breakdown of colloid filtration theory: Role of the secondary energy minimum and surface charge heterogeneities, *Langmuir*, *21*, 841–852.

Tufenkji, N., and M. Elimelech (2005b), Spatial distributions of Cryptosporidium oocysts in porous media: Evidence for dual mode deposition, *Environ. Sci. Technol.*, *39*, 3620–3629.

Verwey, E. J. W., and J. Th. G. Overbeek (1948), *Theory of the Stability of Lyophobic Colloids*, Elsevier, Amsterdam.

Wan, J. M., and T. K. Tokunaga (2002), Partitioning of clay colloids at air–water interfaces, *J. Colloid Interface Sci.*, *247*, 54–61.

Xu, S., B. Gao, and J. E. Saiers (2006), Straining of colloidal particles in saturated porous media, *Water Resour. Res.*, *42*, W12S16, doi:10.1029/2006WR004948.

Yao, K. M., M. T. Habibian, and C. R. O'Melia (1971), Water and waste water filtration—Concepts and applications, *Environ. Sci. Technol.*, *5*, 1105–1112.

Yoon, J. S., J. T. Germaine, and P. J. Culligan (2006), Visualization of particle behavior with a porous medium: Mechanisms for particle filtration and retardation during downward transport, *Water Resour. Res.*, *42*, W06417, doi:10.1029/2004WR003660.

Yuan, H., and A. A. Shapiro (2011), A mathematical model for non-monotonic deposition profiles in deep bed filtration systems, *Chem. Eng. J.*, *166*, 105–115.

Zhang, P., W. P. Johnson, T. D. Scheibe, K. Choi, F. C. Dobbs, and B. J. Mailloux (2001), Extended tailing of bacteria following breakthrough at the Narrow Channel Focus Area, Oyster, Virginia, *Water Resour. Res.*, *37*, 2687–2698, doi:10.1029/2000WR000151.

S. A. Bradford, US Salinity Laboratory, USDA, ARS, 450 West Big Springs Road, Riverside, CA 92507, USA. (Scott.Bradford@ars.usda.gov)

J. Simunek and S. Torkzaban, Department of Environmental Sciences, University of California, 2320 Geology, Riverside, CA 92521, USA.